We are IntechOpen,
the world's leading publisher of Open Access books
Built by scientists, for scientists

6,900
Open access books available

186,000
International authors and editors

200M
Downloads

154
Countries delivered to

Our authors are among the

TOP 1%
most cited scientists

12.2%
Contributors from top 500 universities

BOOK CITATION INDEX
CLARIVATE ANALYTICS
INDEXED

WEB OF SCIENCE™

Selection of our books indexed in the Book Citation Index
in Web of Science™ Core Collection (BKCI)

Interested in publishing with us?
Contact book.department@intechopen.com

Coherent Structures in the Near Field of Swirling Turbulent Jets and Flames Investigated by PIV and PLIF

Vladimir Dulin, Aleksei Lobasov,
Dmitriy Markovich and Sergey Alekseenko

Additional information is available at the end of the chapter

Abstract

The results of the experimental study of coherent flow structures in turbulent jets with different swirl rates are reported. The focus is placed on analysis of their impact on mixing of a passive scalar in the jets and on regular flame front deformations during combustion of fuel-lean and fuel-rich methane/air mixtures in case of a strongly swirling jet with vortex breakdown. The measurements are performed by applying simultaneously the particle image velocimetry (PIV) and planar laser-induced fluorescence (PLIF) techniques (acetone and HCHO for the nonreacting and reacting flows, respectively). The PIV data are processed by a proper orthogonal decomposition (POD), and the PLIF data are conditionally sampled according to the correlation coefficients of the velocity POD modes. The coherent velocity fluctuations are associated with regular patterns in the concentration fluctuation fields and flame front deformations. These patterns correspond to unsteady mixing by large-scale vortex structures in the outer mixing layer and also to variations of the entrainment rate for the flows with swirl.

Keywords: swirling jet, mixing, swirling flame, vortex breakdown, coherent structures, precessing vortex core

1. Introduction

Swirl is often superimposed to jet flows to promote mixing and heat and mass transfer in the initial region of the flow [1–4]. Whereas ring-like vortices are formed in the shear layer of the nonswirling and weakly swirling jets, helical vortex structures are formed in the mixing layer of strongly swirling jets and considered to enhance mixing [4–8]. When the swirl rate exceeds a certain critical value, a breakdown of the vortex occurs in swirling jets [6, 7, 9–12]. The vortex

breakdown corresponds to formation of a wake region or recirculation zone at the jet axis and intensifies mixing even more via unsteady flow dynamics. The low velocity region at the low-pressure core of the swirling flow provides favorable local conditions for successful ignition and stable combustion of flames [1, 13]. Thus, swirling jet flows are often implemented in combustion chambers and furnaces.

Structure of swirling flows with combustion has been studied extensively in a number of experiments. Heat release and local density decrease during combustion strongly affect the shape of the recirculation zone [14, 15]. Hot combustion products tend to concentrate at the vortex core and are captured by the central recirculation zone [16–20]. Moreover, combustion is known to induce vortex breakdown, which was absent for the nonreacting flow before ignition of the flame [21–23]. Besides, amplitude of the vortex core precession is found to be suppressed by combustion in some studies, whereas in the other, it was not strongly affected [24, 25]. Detailed experimental data on flow structure of swirling flows with combustion is necessary for verification of numerical simulations, which are currently performed with eddy-resolving methods [26–31].

Presently, the impact of unsteady swirling flow dynamics, such as precession of the vortex core, which is found to produce intensive velocity and pressure pulsations in jets with vortex breakdown, on unsteady combustion is not completely understood [32]. In particular, the impact of the precessing vortex core on flame instabilities and unsteady operation of swirl-stabilized combustors is still a debated issue [33]. Ruith et al. [11] and Liang and Maxworthy [7] suggest that formation of the recirculation zone triggers a global instability mode, which results in unsteady dynamics of swirling jets, related to intensive velocity and pressure fluctuations during precession of the swirling vortex core near the nozzle. Oberleithner et al. [12] have suggested that during the increase of the jet swirl rate the central recirculation zone first appears in an intermittent manner and then remains permanently. Further increase of the swirl rate gives rise to a global flow instability to a helical mode, corresponding to precession of the swirling jet.

From conditionally sampled velocity measurements by the laser Doppler velocimetry technique, Cala et al. [34] have detected a coherent structure in a high-swirl jet, consisted of a spiraling vortex core and secondary helical large-scale vortex structures in the inner and outer mixing layers. Later, similar structures were detected from 2D particle image velocimetry (PIV) measurements for high-swirl nonreacting jets [35, 36] and flames [37–39]. Later, the presence of double-helical coherent vortex structure was confirmed from direct 3D PIV measurements in [8, 40]. However, there is still a lack of experimental studies on mixing in swirling turbulent jets and quantitative analysis of large-scale vortices contribution to this process.

Dynamics of flow and flame in swirl combustors is studied successfully by combination of PIV and planar laser-induced fluorescence (PLIF) of OH* (see [41, 42]). The hydroxyl radical OH*, produced in flame front and present in hot combustion products, is commonly used for tracking of the front. Stöhr et al. [42] have found that large-scale vortices improve mixing between the combustion products and reactants. Meanwhile, Boxx et al. [41] have observed events of local flame extinction during its interaction with large-scale vortices in the high-swirl flow. Nevertheless, further detailed analysis of the reaction zone shape correlations with large-scale flow motions in swirling jet flows is desirable.

Formaldehyde (HCHO) is an important combustion intermediate, occurring in lower-temperature regions of hydrocarbon-fueled flames. It plays an important role in several combustion processes, including fuel oxidation and autoignition. It appears in the initial step of the $HCHO \rightarrow HCO \rightarrow CO$ oxidation pathway of conventional hydrocarbons [43]. High concentration of HCHO specifies preheat zone of hydrocarbon flames. One of the most prevalent strategies for HCHO PLIF measurements is the excitation of 4^1_0 transition by using the third harmonic of Nd:YAG laser radiation at 355 nm [44].

The aim of the current study is to analyze the impact of large-scale vortex structures on mixing in turbulent jets with different swirl rates on the basis of the combined PIV and PLIF measurements and to reveal regular flame front deformations during combustion of fuel-lean and fuel-rich flames in the swirling jet with high swirl rate and vortex breakdown.

2. Experimental setup and data processing

Measurements were carried out for swirling jets and premixed methane/air flames at the atmospheric pressure. The flow was organized in an open combustion rig by using a contraction axisymmetric nozzle with a changeable vane swirler installed inside to generate jet flows with swirl. The outlet diameter of the nozzle was $d = 15$ mm (see [37] for the details). The swirl rate S was estimated based on the geometric parameters of the swirler [1]:

$$S = \frac{2}{3} \left(\frac{1 - (d_1/d_2)^3}{1 - (d_1/d_2)^2} \right) \tan(\psi) \tag{1}$$

where $d_1 = 7$ mm is the diameter of the center body supporting the vanes, $d_2 = 27$ mm is the external diameter of the swirler, and ψ is the vanes inclination angle relative to the axis. Three cases of the swirl rate are considered, viz., nonswirling jet without swirler ($S = 0$) and swirling jets for $\psi = 30, 45,$ and $55°$, corresponding to $S = 0.41, 0.7,$ and 1.0, respectively, whereas the critical value for the vortex breakdown in jet flows is $S \approx 0.6$ [14, 45–47].

The air flow was supplied from a pressure line, and its flow rate was precisely controlled by mass flow meters (Bronkhorst). To introduce acetone vapor into the nonreacting jet flows, a part of the air flow was bubbled through liquid acetone, contained in a thermostabilized container at a fixed temperature. The concentration of the acetone in the jet was below 3%. The Reynolds number based on the flowrate of air was fixed as 5000 (bulk velocity for the air jet was $U_0 = 5.0$ m/s).

For the reacting flows, the container with acetone was not used. Instead, the air was premixed with methane, supplied by another set of Bronkhorst mass flow meters. The equivalence ratio φ of the methane/air mixtures issued from the nozzle was equal to 0.7 and 2.5. To provide PIV measurements, the jet flow was seeded by 0.5 μm TiO_2 particles. The surrounding air was seeded by using a fog generator.

A sketch of the PIV/PLIF experimental setup is shown in **Figure 1**. Two CCD PIV cameras (ImperX IGV-B2020) were oriented horizontally as shown in **Figure 1**. The cameras were
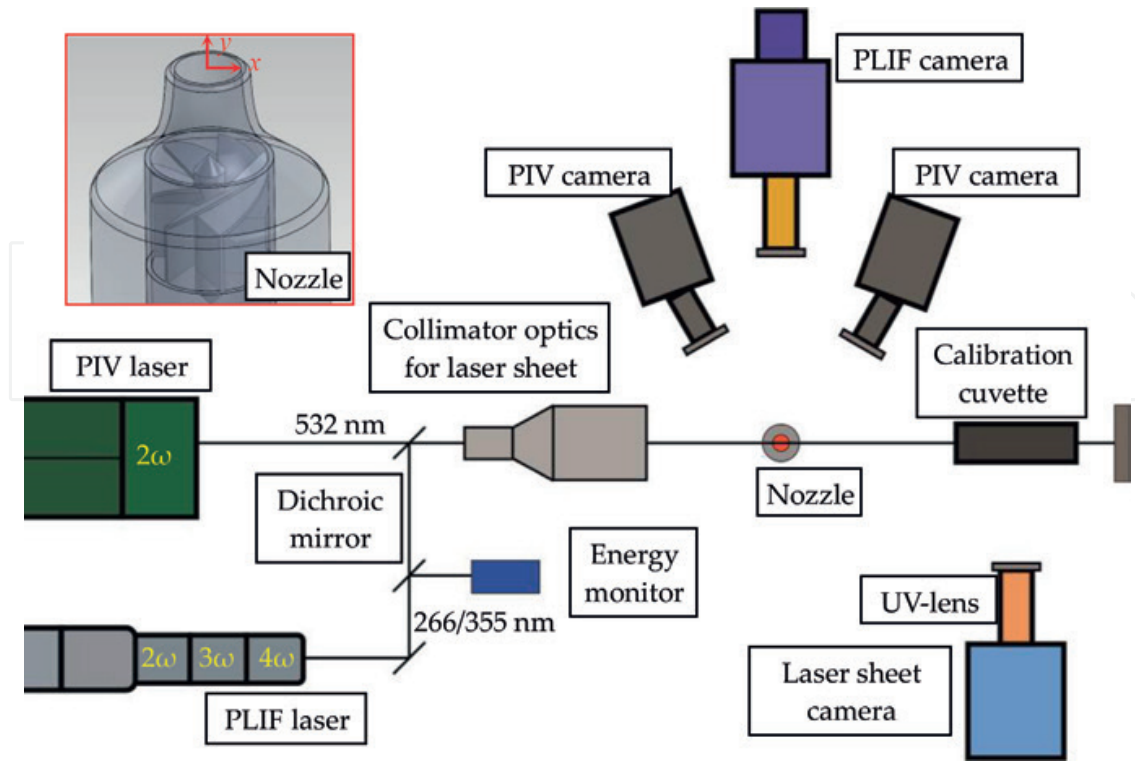
Figure 1. Sketch of the PIV/PLIF setup and geometry of the nozzle (inset).

equipped with narrow band-pass optical filters (532 ± 10 nm). A double-head Nd:YAG laser (Quantel EverGreen) was used to illuminate the tracer particles in the central plane of the flow for the PIV measurements. Duration of each laser pulse was approximately 10 ns. The time interval between two PIV laser pulses for the reacting flows was 35 μs.

The velocity fields were evaluated by an adaptive iterative cross correlation algorithm with continuous image shift and deformation (see [48] for the definition), included an in-house software "ActualFlow." The final size of the interrogation areas was 32×32 pixels. The spatial overlap rate between the neighbor interrogation areas was 50%. Calibration of the stereo PIV and PLIF cameras was performed by using a plane calibration target and third-order polynomial transform. This was done by processing images of the calibration target placed in five different positions in the normal-to-plane direction with the step of 0.5 mm. In addition, to minimize the calibration error, an iterative correction procedure of possible misalignment between the laser sheet and the target plane was applied [49]. For almost the entire measurement domain, the mismatch between the actual marker locations on the target and their coordinates in the obtained calibration model was below 1 pixel.

The fourth harmonic (266 nm) of a pulsed Nd:YAG laser (Quantel Brilliant B) was used for excitation of the acetone fluorescence. During excitation of the HCHO fluorescence (4^1_0 transition of A–X band) for the reacting flows, the third harmonic (355 nm) of the same laser was used. Duration of each laser pulse was approximately 10 ns. The laser beams for the PLIF and PIV systems were combined by using a dichroic mirror and converted into a collimated laser sheet with the width of 50 mm. The laser sheet thickness was below 0.8 mm in the measurement region.

Fluorescence of HCHO and acetone was collected by a system of UV-sensitive image intensifier (LaVision IRO, photocathode S20 multialkali provided quantum efficiency about 25% for wavelengths in UV spectral region) and sCMOS camera (LaVision Imager sCMOS, 16 bit images with resolution of 2560 × 2160 pixels), equipped with a UV lens (100 mm, f# = 2.8) and band-pass optical filter. The exposure time for each PLIF image was 200 ns. The PLIF signal was collected almost in the center of the time interval between two pairs of the PIV laser pulses.

The raw PLIF images contained different types of systematic and random errors. The systematic errors were produced by spatially nonuniform laser sheet intensity, nonuniform spatial sensitivity of the photocathode and CCD, dark current of the sensors, and background signal (due to possible reflections, etc.). A set of post-processing algorithms were applied to the PLIF images to remove the dark current and background intensity and to correct for the spatial nonuniformity of the laser sheet intensity and sensitivity of the sensors. An additional ICCD camera (PCO DicamPro) was used to monitor the spatial distribution of energy in each pulse of the PLIF lasers by using a quartz cuvette filled with uniform solution of a fluorescent dye (Rhodamine 6G).

Typical magnification of the PIV and PLIF systems was 29.9 and 35.0 pixels per mm, respectively. The optical resolution of the PLIF system corresponded to a Gaussian-type smoothing with the full width at the half maximum of approximately 15 pixels. The resolution was evaluated based on a "knife-edge technique" similar to that in [50]. To fit grids of the PIV and PLIF data, the latter was spatially averaged over domains with the size of 0.96 mm and 50% overlap rate. The laser sheet thickness in the region of interest for both systems was approximately 0.8 mm.

To reveal coherent structures in the flows, the fluctuating velocity data set $W = [\mathbf{u}'(\mathbf{x}, t_1)\ldots\mathbf{u}'(\mathbf{x}, t_N)]$ for each flow case was processed by a snapshot proper orthogonal decomposition (POD) [51]. POD is based on a singular value decomposition:

$$\mathbf{u}'(\mathbf{x}, t_k) = \sum_{q=1}^{N} \alpha_q(t_k)\sigma_q\boldsymbol{\varphi}_q(\mathbf{x}) \text{ or in a matrix form } W = U\Sigma V^H, \tag{2}$$

$$\text{where } \int_\Omega \boldsymbol{\varphi}_i\boldsymbol{\varphi}_j d\mathbf{x} = \delta_{ij} \text{ and } \frac{1}{N}\sum_{k=1}^{N} \alpha_i(t_k)\alpha_j(t_k) = \delta_{ij} \tag{3}$$

Each set of the fluctuating velocity fields $\mathbf{u}'(\mathbf{x}, t_k)$ is represented as a finite series of the products of the spatial orthonormal basis functions $\boldsymbol{\phi}_q$ ($U = [\boldsymbol{\phi}_1\ldots\boldsymbol{\phi}_N]$) with nondimensional temporal coefficients α_q (corresponding to the conjugate transpose of a matrix V that is composed of the right-singular vectors of W) and singular values σ_q ($\Sigma = \text{diag}[\sigma_1\ldots \sigma_N]$). N is the number of the snapshots in the set. The singular values characterize the amplitude (square root of the kinetic energy of the velocity fluctuations) of each POD mode in the data sequence and are equal to square root of the eigenvalues of the covariance matrix WW^H. For the used snapshot POD method, the POD modes can be represented as:

$$\boldsymbol{\varphi}_q(\mathbf{x}) = \sum_{k=1}^{N} a_q^k \mathbf{u}'(\mathbf{x}, t_k)\sigma_k^{-1} \text{ or } U = W\Sigma^{-1}V \qquad (4)$$

To reveal coherent structure effect on mixing and flame front deformation, fluctuations $I'(\mathbf{x}, t)$ of the PLIF data are conditionally sampled according to the temporal coefficients a^k_q (from matrix V) of the POD modes:

$$c_q(\mathbf{x}) = \frac{u_{rms}}{I_{rms}} \sum_{k=1}^{N} a_q^k I'(\mathbf{x}, t_k)\sigma_k^{-1}, \text{ where } u_{rms}^2 = \int_\Omega \mathbf{u}'^2 d\mathbf{x} \text{ and } I_{rms}^2 = \int_\Omega I'^2 d\mathbf{x} \qquad (5)$$

3. Results

3.1. Swirling jets without combustion

Figure 2 shows the time-averaged velocity fields and turbulent kinetic energy for the nonreacting jets. The core of the nonswirling jet ($S = 0$) is surrounded by the circular mixing layer, where velocity fluctuations grow downstream. For the case $S = 0.41$ (referred to as low-swirl jet), a wake region is formed at the jet axis, where the average axial velocity remains positive. The velocity fluctuations for the outer mixing layer of the low swirl are considerably greater. Also, their intensity at the onset of the central wake region reached 35% of U_0. For the cases $S = 0.7$ and 1.0 (referred to as high-swirl jets), the black solid line surrounds the region with negative values of the mean axial velocity, corresponding to the central recirculation zone.

Thus, there are two mixing layers in the flow of the swirling jets, viz., the inner mixing layer between the annular swirling jet and the central recirculation zone/wake region and the outer mixing layer between the jet and the surrounding air. The swirl results in a greater opening angle for the jet. It is increased from approximately 11 to 37° (half angle) for the considered range of swirl rates.

The normalized spatial distributions of the time-averaged acetone concentration are shown in **Figure 3**. The swirl results in a faster mixing of the jet with the surrounding air. The contour lines show values of the local variance of the concentration. Thus, the concentration fluctuates in the outer mixing layer. The swirl decreases the length of the mixing region, viz., it is less than one nozzle diameter for the case $S = 1.0$. Thus, the flow swirl and vortex breakdown dramatically promote the mixing.

Examples of the instantaneous velocity and concentration fields, measured simultaneously and plotted in **Figure 4**, show an effect of large-scale vertical structures on turbulent mixing in the studied jets. The large-scale vortex structures are visualized by regions with positive values of a 2D modification (Eq. (6)) of Q-criterion [52], viz., $Q^{2D} > 5U_0^2 d^{-2}$. For the nonswirling jet, it is expected that the vortex cores in the outer mixing layer correspond to ring-like vortices. They engulf and entrain the surrounding air, whereas the jet core remains almost unmixed. For the low-swirl jet, the acetone spreads faster into the surrounding air and the mixing is more efficient.
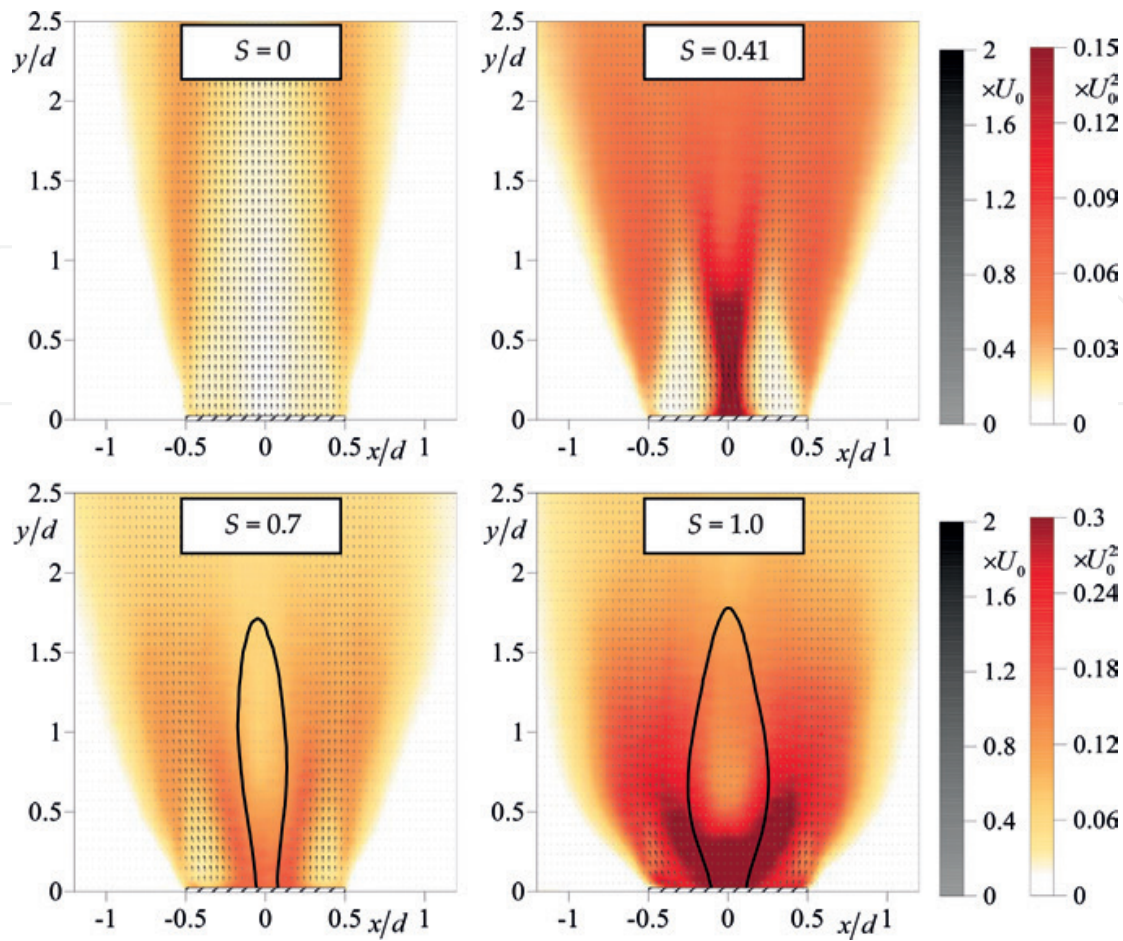
Figure 2. Time-averaged velocity fields and distributions of the turbulent kinetic energy for nonreacting swirling jets. Black solid line includes regions with negative axial velocity.

$$Q^{2D} = -\frac{1}{2}\frac{\partial u_x}{\partial x}\frac{\partial u_x}{\partial x} - \frac{1}{2}\frac{\partial u_y}{\partial y}\frac{\partial u_y}{\partial y} - \frac{\partial u_x}{\partial y}\frac{\partial u_y}{\partial x}. \tag{6}$$

Whereas the vortex structures present both in the inner and outer mixing layers of the low-swirl jet, their contribution to the mixing near the wake region is small. During the mixing in the high-swirl jets, some amount of the surrounding air is captured by the central recirculation zone and mixed with annular jet, issued from the nozzle. Thus, the contribution of large-scale vortex structures to the jet dilution in the inner mixing layer increases with swirl rate.

To reveal coherent structures in the flows and to analyze their contribution to mixing, POD is applied to the sets of the measured velocity fields. The POD spectra of the velocity fluctuations in the nonreacting jets for different swirl rates are shown in **Figure 5**. For the high-swirl jets with vortex breakdown, there are two most energetic modes. They contain approximately 9 and 16% of the spatial-averaged turbulent kinetic energy for the cases of $S = 0.7$ and 1.0, respectively, whereas the energy of rest modes is below 2%. Values of the temporal coefficients for the first two modes for $S = 1.0$, shown in **Figure 5**, are scattered around a circle-like figure, indicating that these modes are statistically correlated.
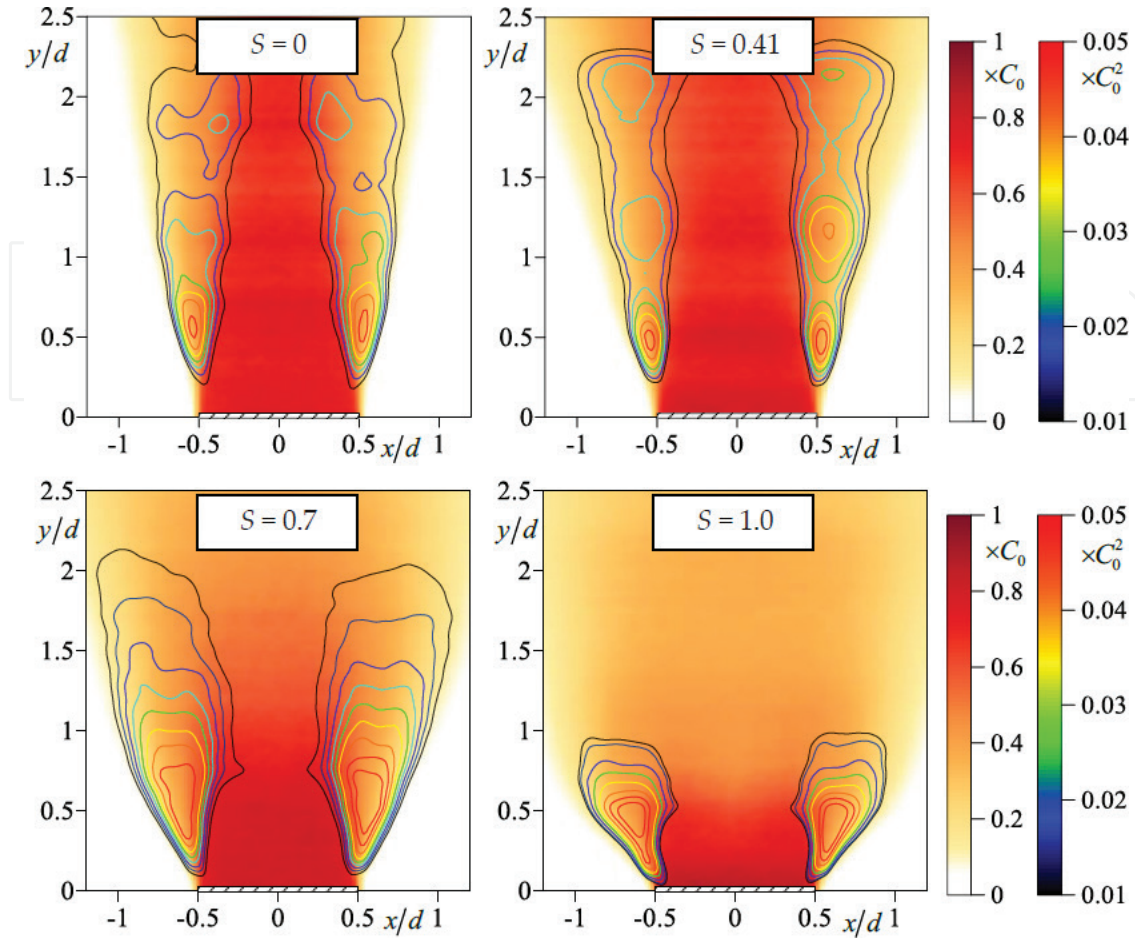
Figure 3. Time-averaged values and variance of the passive scalar concentration for nonreacting turbulent jets with different swirl rate.

Spatial distributions of the first four POD modes for the nonswirling jet with corresponding conditionally sampled fluctuations of the acetone concentration are shown in **Figure 6**. The distributions of the fluctuations correspond to growing downstream vortex structures and expanding traveling waves of the concentration fluctuations. The first and second POD modes appear to be shifted by $\pi/2$ phase and are expected to be related to growing downstream ring-like vortices. The third and fourth modes are likely to be associated with pairing process of these ring-like vortices at approximately $1.5d$ downstream the nozzle exit and related modulation of amplitude of the subsequent vortices upstream via pressure feedback mechanism [53].

For the low-swirl jet (see **Figure 7**), the first POD mode is related to oscillations of the axial velocity near the central wake, which is in agreement with the scenario of the vortex breakdown by Oberleithner et al. [12], where formation of the permanent recirculation zone is preceded by an intermittent formations of the reverse flow at the jet axis. It is found that such fluctuations are coherent with large-scale variation of the entrainment rate downstream. The second POD mode is presumably related to precession of the vortex core upstream the wake region and also correlated with downstream variation concentration fluctuations. The third and fourth POD modes correspond to traveling waves of the concentration fluctuations in the outer mixing layer, produced by growing downstream large-scale toroidal vortex structures.
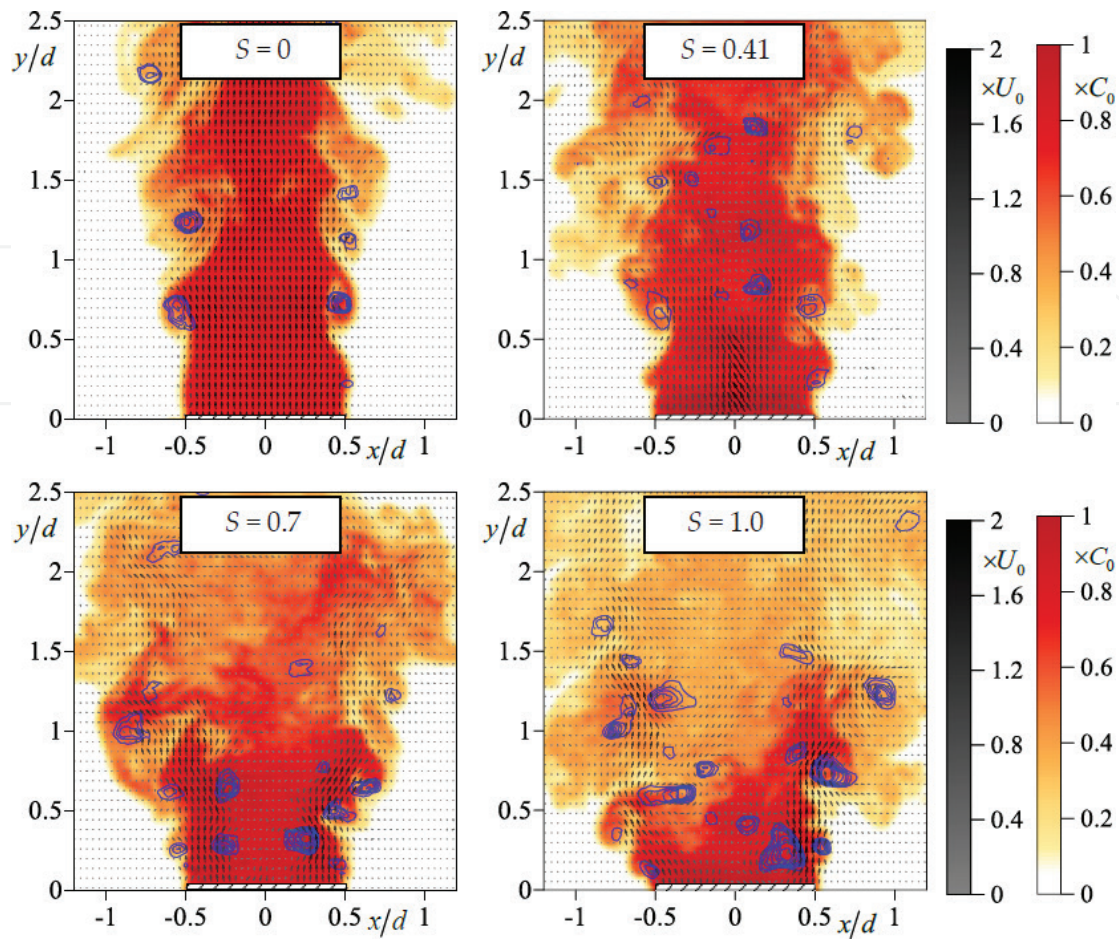
Figure 4. The instantaneous velocity and concentration snapshots for turbulent jets with different swirl rate. Large-scale vortical structures are visualized by regions with positive Q-criterion ($Q^{2D} \geq 5U_0^2 d^{-2}$ with the step of $2.5U_0^2 d^{-2}$).
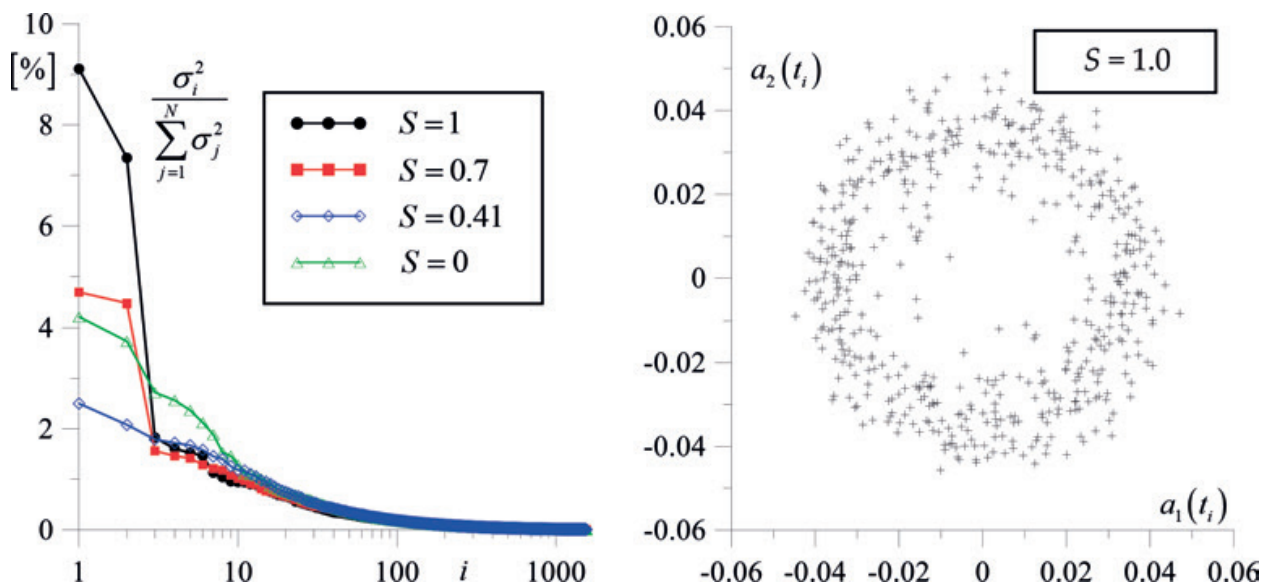

Figure 5. POD spectra for nonreacting jets and temporal coefficients for the first two POD modes for the high-swirl jet.
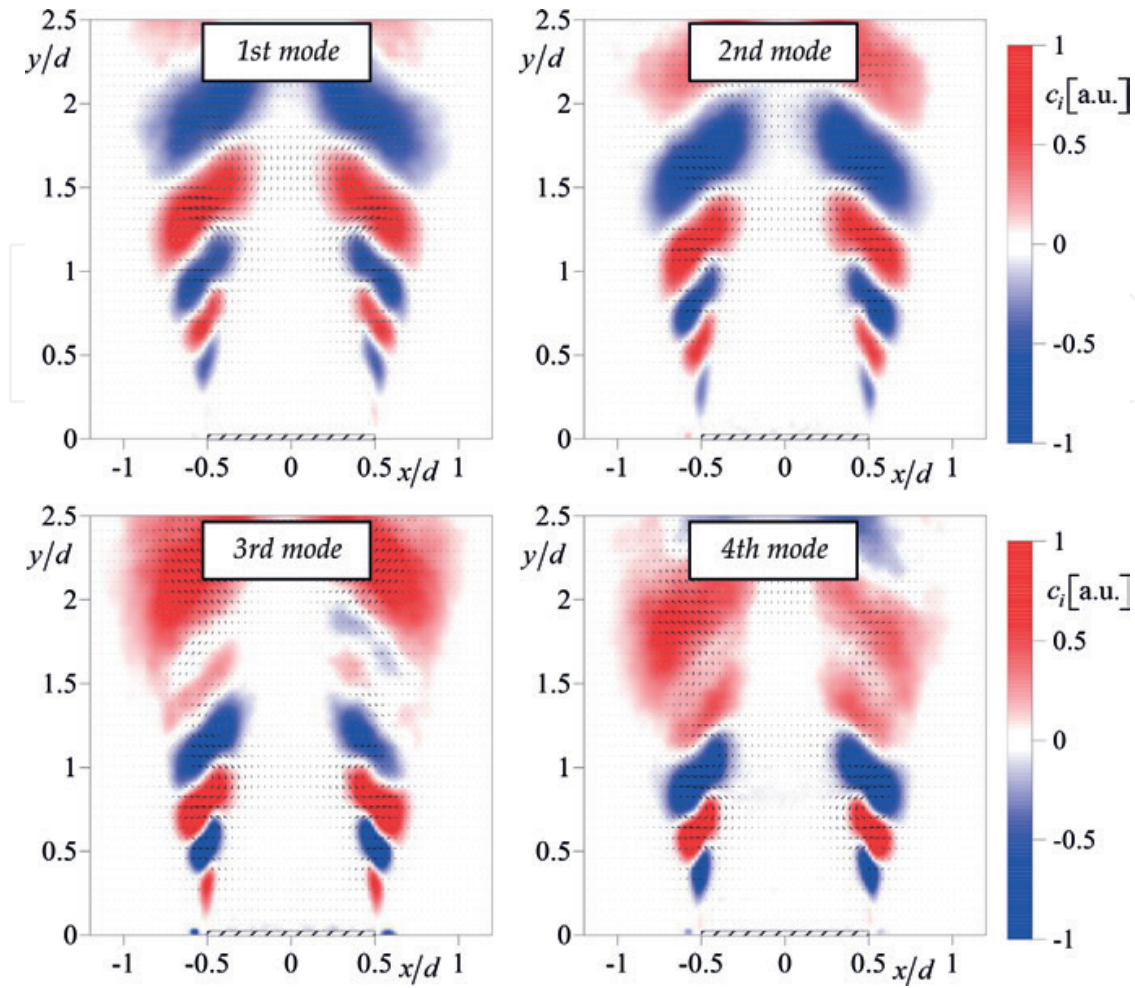
Figure 6. First four POD modes of the velocity fluctuations and corresponding conditionally sampled fluctuations of the concentration for a nonswirling jet ($S = 0$).

Figures 8 and **9** show the first four POD modes for the high-swirl jets for $S = 0.7$ and 1.0, respectively. The first two POD modes correspond to transverse velocity fluctuations around the nozzle exit, correlated with the velocity fluctuations in the inner and outer mixing layer. The concentration fluctuations related to these modes correspond to expanding downstream traveling waves. In analogy to the nonswirling jet, the first and second POD modes appear to be shifted by the phase of $\pi/2$. The main difference between the cases $S = 0.7$ and 1.0 is that in the latter case the coherent fluctuations of the concentration take place both in the inner and outer mixing layers.

The results for the high-swirl jets are in agreement with the conclusions of the previous 2D PIV study in [37], where it was proposed that these two POD modes correspond to two orthogonal cross planes of a single rotating coherent structure, consisting of a precessing spiraling vortex core (in the inner mixing layer) and a secondary helical vortex structure (in the outer mixing layer). This assumption was later supported in studies of the nonreacting swirling jets by 3D PIV [8]. Thus, the outer helical vortex of the coherent structure produces regular large-scale structures in the spatial distributions of the concentration fluctuations.
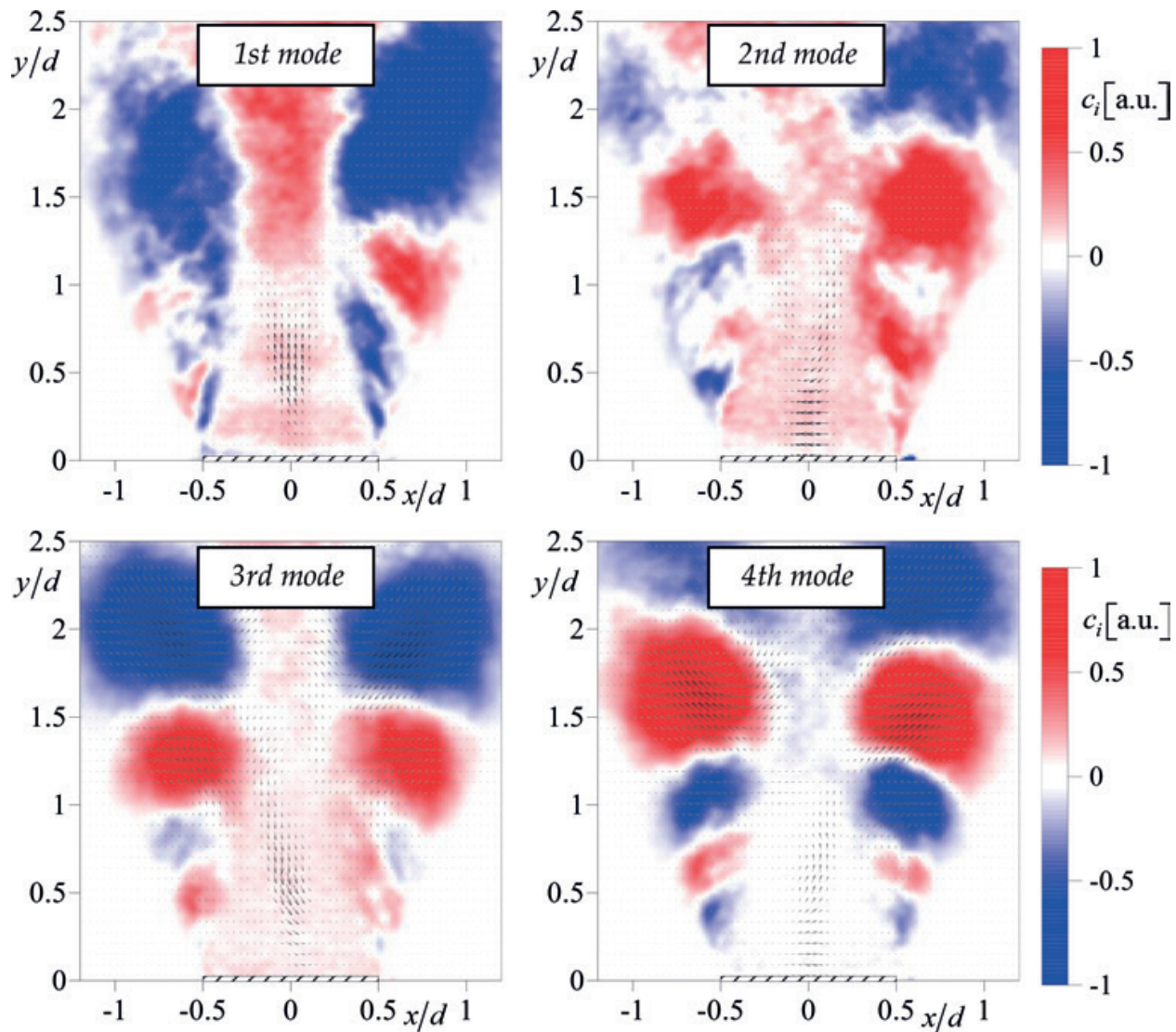
Figure 7. First four POD modes of the velocity fluctuations and corresponding conditionally sampled fluctuations of the concentration for a low swirling jet ($S = 0.41$).

3.2. High-swirl jets with combustion

Figure 10 shows the photograph, time-averaged velocity field, and HCHO PLIF signal for the high swirling jet with combustion. Two flame cases are considered, viz., combustion of the fuel-lean and fuel-rich mixtures with the equivalence ratio of $\varphi = 0.7$ and 2.5, respectively. The black solid lines in the time-averaged velocity fields surround regions with negative values of the mean axial velocity, corresponding to the central recirculation zone. Note that the shape of the recirculation zone for these two cases is very similar. In general, there are two mixing layers in the flows as it is the case for the nonreacting high-swirl jet.

For the fuel-lean flame ($\varphi = 0.7$), the annular jet flow envelopes the central recirculation zone, containing a weak reverse flow. According to the PLIF signal, the flame front is located in the inner mixing layer of the jet flow. On average, the combustion of the fuel-rich mixture takes
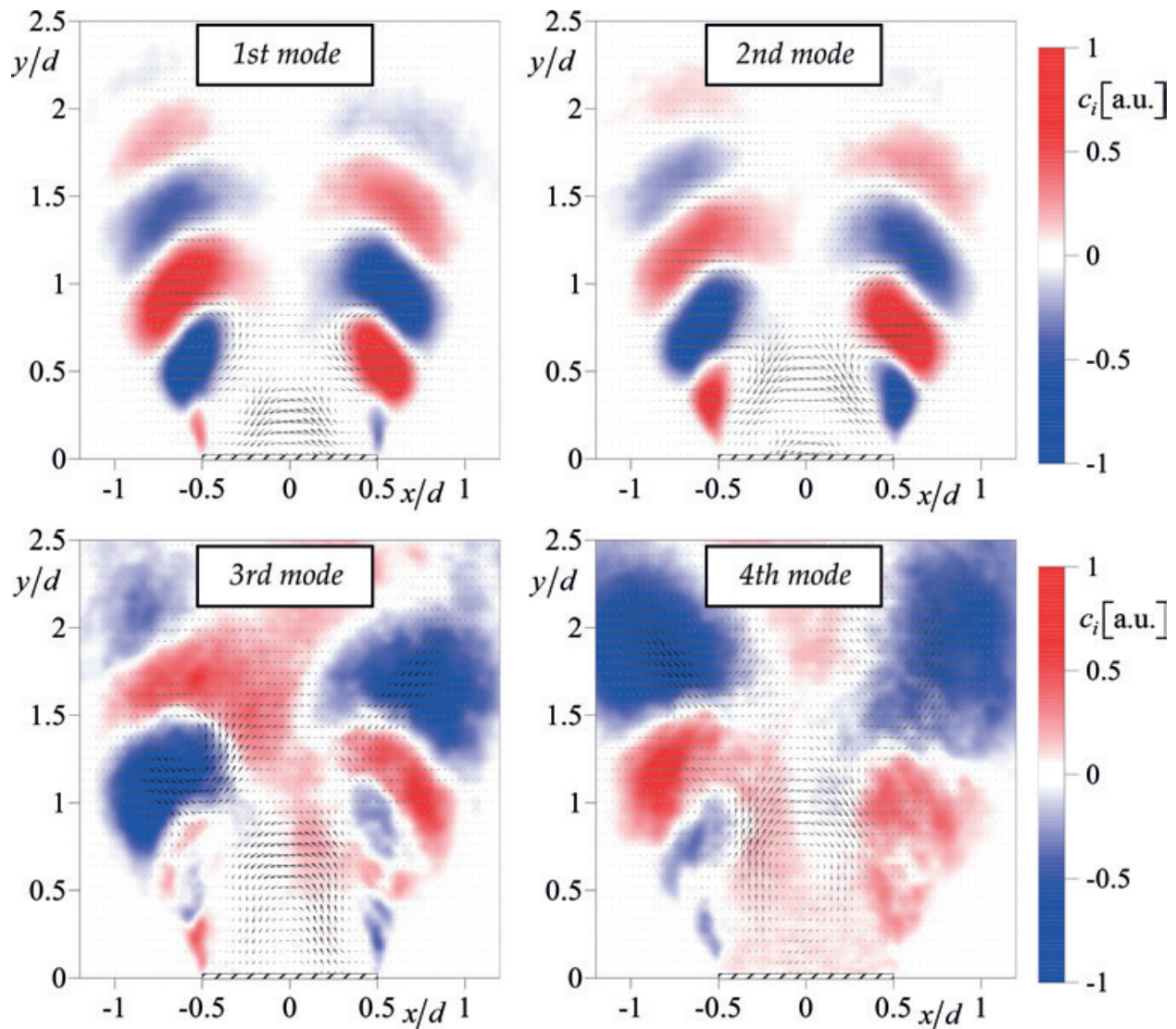
Figure 8. First four POD modes of the velocity fluctuations and corresponding conditionally sampled fluctuations of the concentration for a high swirling jet ($S = 0.7$).

place both in the outer (above $0.7d$ from the nozzle exit) and in the inner (around the central recirculation zone) mixing layers.

Figure 11 shows the instantaneous snapshots of the velocity and HCHO PLIF signal for the high-swirl jets with combustion. Large-scale vortex structures are visualized by the 2D modification of Q-criterion. For the fuel-lean mixture, there are pairs of large-scale vortices, which corrugate the flame front (indicated by arrows). The vortices in the pair envelope the flame front from opposite sides (one vortex is located in the inner mixing layer, whereas another one is in the outer mixing layer). In the previous study of [39], it was suggested that these vortex pairs are cross sections of two helical vortex structures with one present in the inner mixing layer and another one located in the outer mixing layer.

The instantaneous velocity and HCHO PLIF data for the fuel-rich flame illustrate that the flame front surrounds the central reticulation zone with a complex shape, corresponding to downward flow between the large-scale vortex structures in the inner mixing layer. The flame
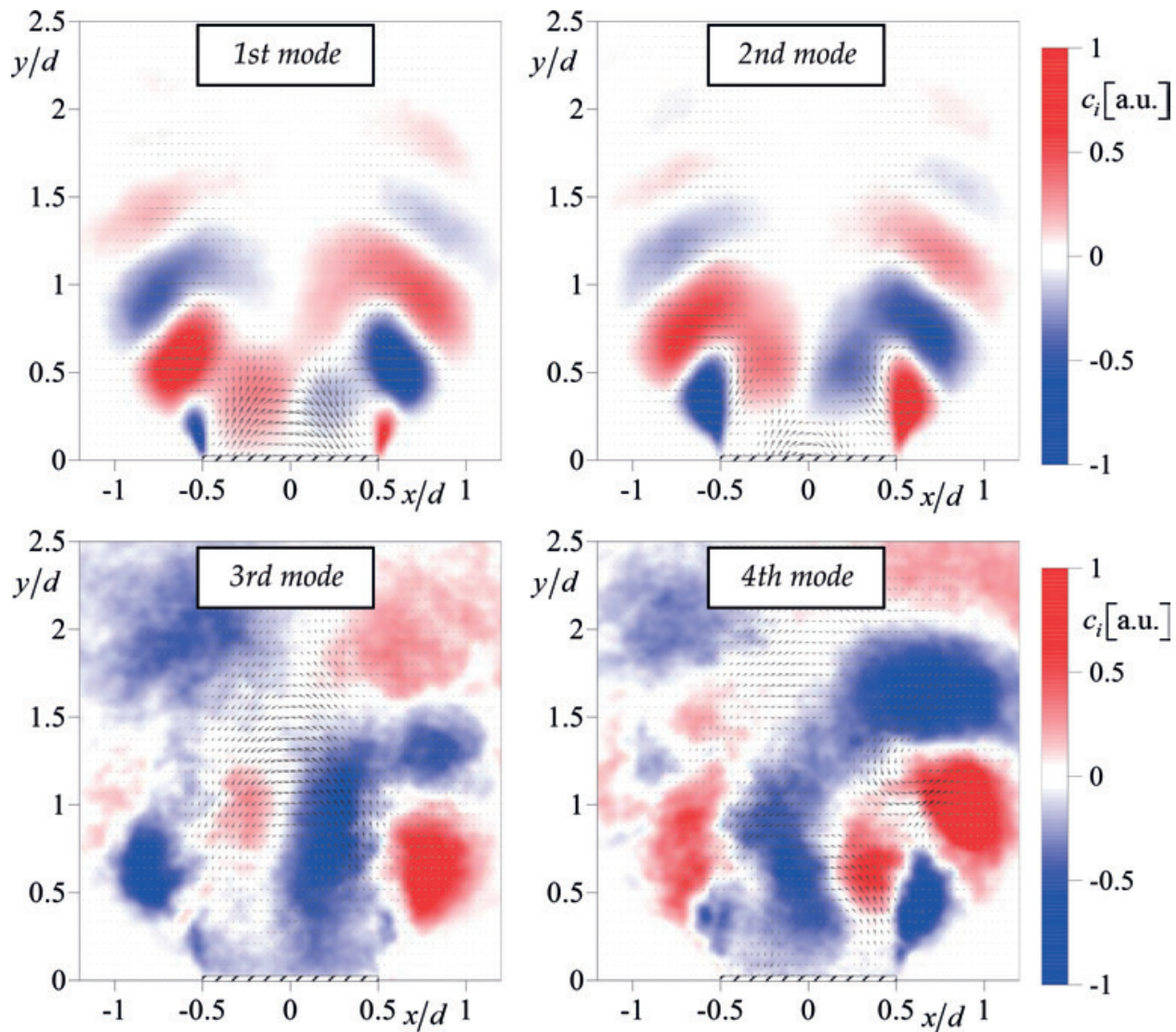
Figure 9. First four POD modes of the velocity fluctuations and corresponding conditionally sampled fluctuations of the concentration for a high swirling jet ($S = 1.0$).

front is also located in the inner mixing layer, where turbulent mixing of the combustion products with the surrounding air is followed by their afterburning. In general, the current PIV/PLIF data supports results of the previous study in [37], where it was concluded that the large-scale helical vortex structure in the outer mixing layer promotes stabilization of the fuel-rich flame via enhanced turbulent mixing.

To reveal coherent structure effect on the flame front shape, the fluctuating velocity data sets are processed by the POD. The POD spectra for the high-swirl flows without combustion and with combustion of the fuel-lean and fuel-rich mixtures are shown in **Figure 12**. For the flows with combustion, amplitude (i.e., the spatial-averaged variance of the velocity fluctuations; note that the density is not constant) of the first two POD modes is considerably smaller in comparison to that for the nonreacting flow. The spatial distributions of the first four POD modes for the reacting flows with $\varphi = 0.7$ and 2.5 are shown in **Figures 13** and **14**, respectively.
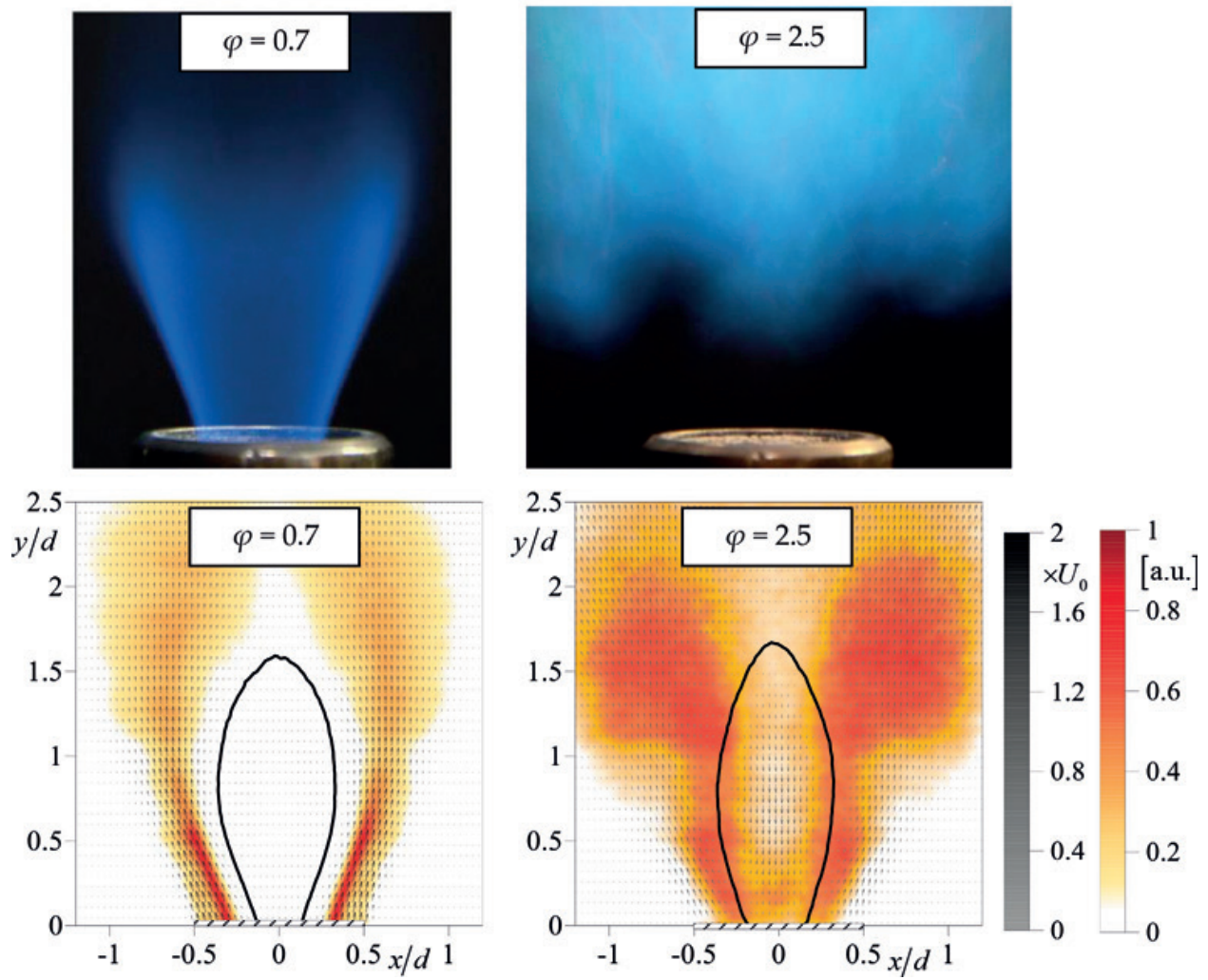
Figure 10. Photographs and time-averaged velocity field and HCHO PLIF for the high-swirl jets (*S* = 1.0) with combustion. Black solid line includes region with negative axial velocity.
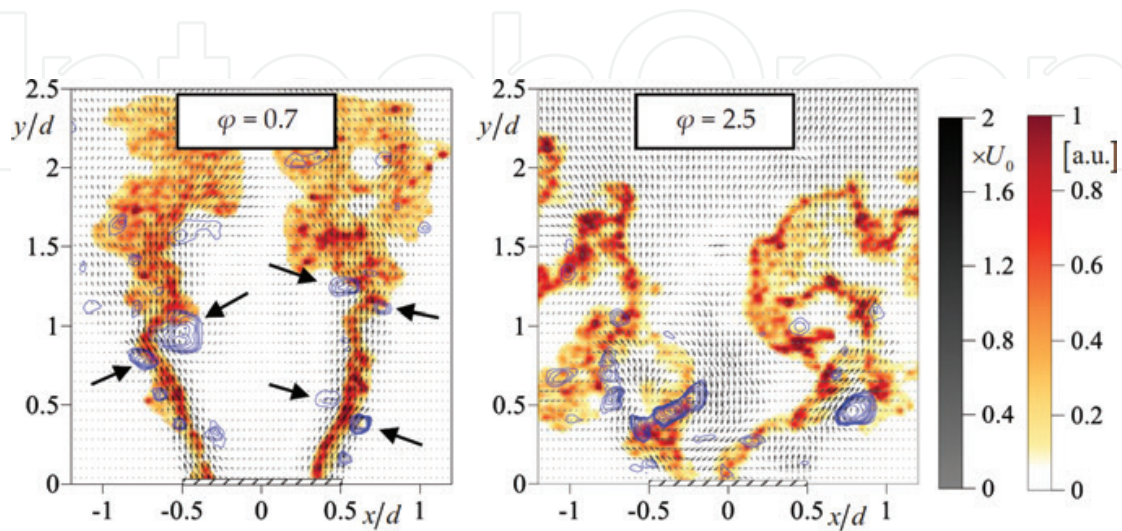

Figure 11. The instantaneous velocity and HCHO PLIF snapshots for turbulent high-swirl jets (*S* = 1.0) with combustion. Large-scale vortical structures are visualized by regions with positive Q-criterion ($Q^{2D} \geq 6U_0^2 d^{-2}$ with the step of $3U_0^2 d^{-2}$).
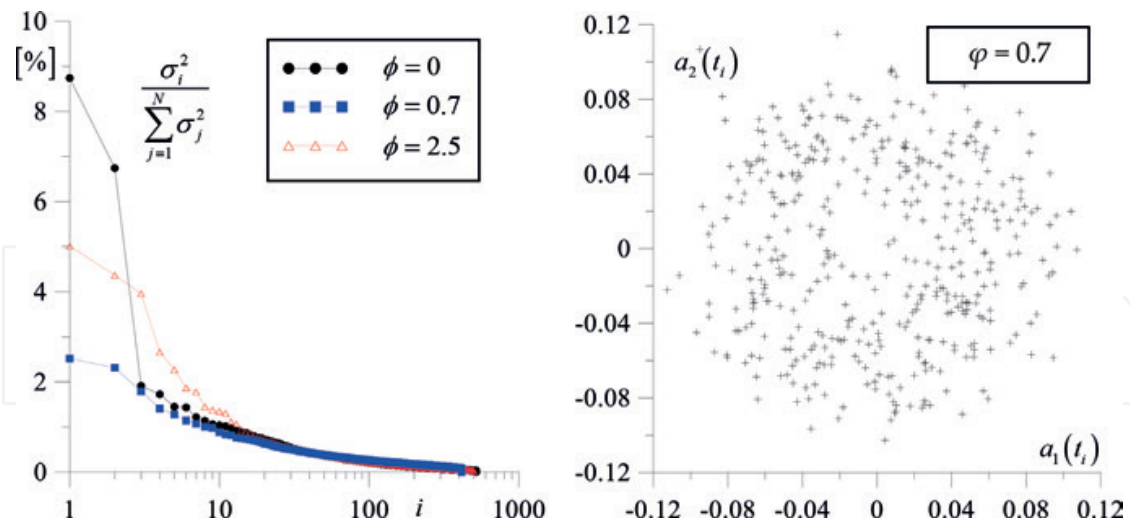
Figure 12. POD spectra for high-swirl jets ($S = 1.0$) with combustion and temporal coefficients for the first two POD modes for the fuel-lean flame.
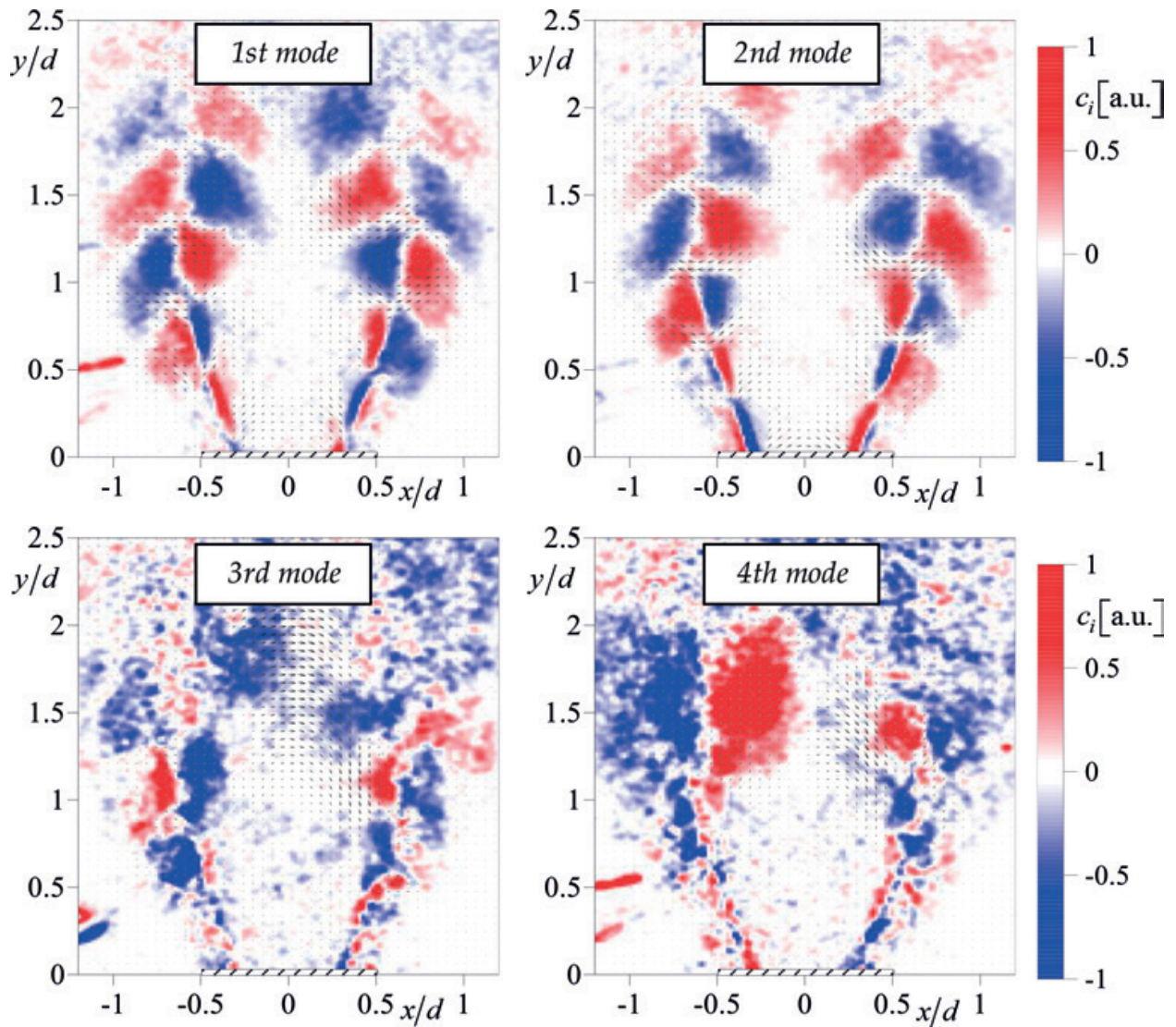

Figure 13. First four POD modes of the velocity fluctuations and conditionally sampled HCHO PLIF fluctuations for a high-swirl fuel-lean flame ($S = 1.0$, $\varphi = 0.7$).

As for the nonreacting flow, the first two POD modes for the fuel-lean flame correspond to coherent velocity fluctuations in the inner and outer mixing layers. The coherent fluctuations of HCHO data correspond to traveling waves along the flame front, which spread down-stream. This correlation is related to the regular flame front deformations during propagation of the large-scale vortex structures. The third and fourth POD modes correspond to the velocity fluctuations in the upper part of the recirculation zone.

For the fuel-rich flame, the spatial structure of the first three POD modes is similar to that reported in [37] for the similar kind of flame, whereas amplitudes of these modes are different. The latter finding is explained by the different field of view in the present and previous experiments. Despite coherent velocity fluctuations in the mixing layers, correlated with the transverse flow movement at the nozzle exit, strong, almost axisymmetric variation of the longitudinal velocity takes place in the outer mixing later, induced by the buoyancy force and resulted in an unsteady entrainment of surrounding air.
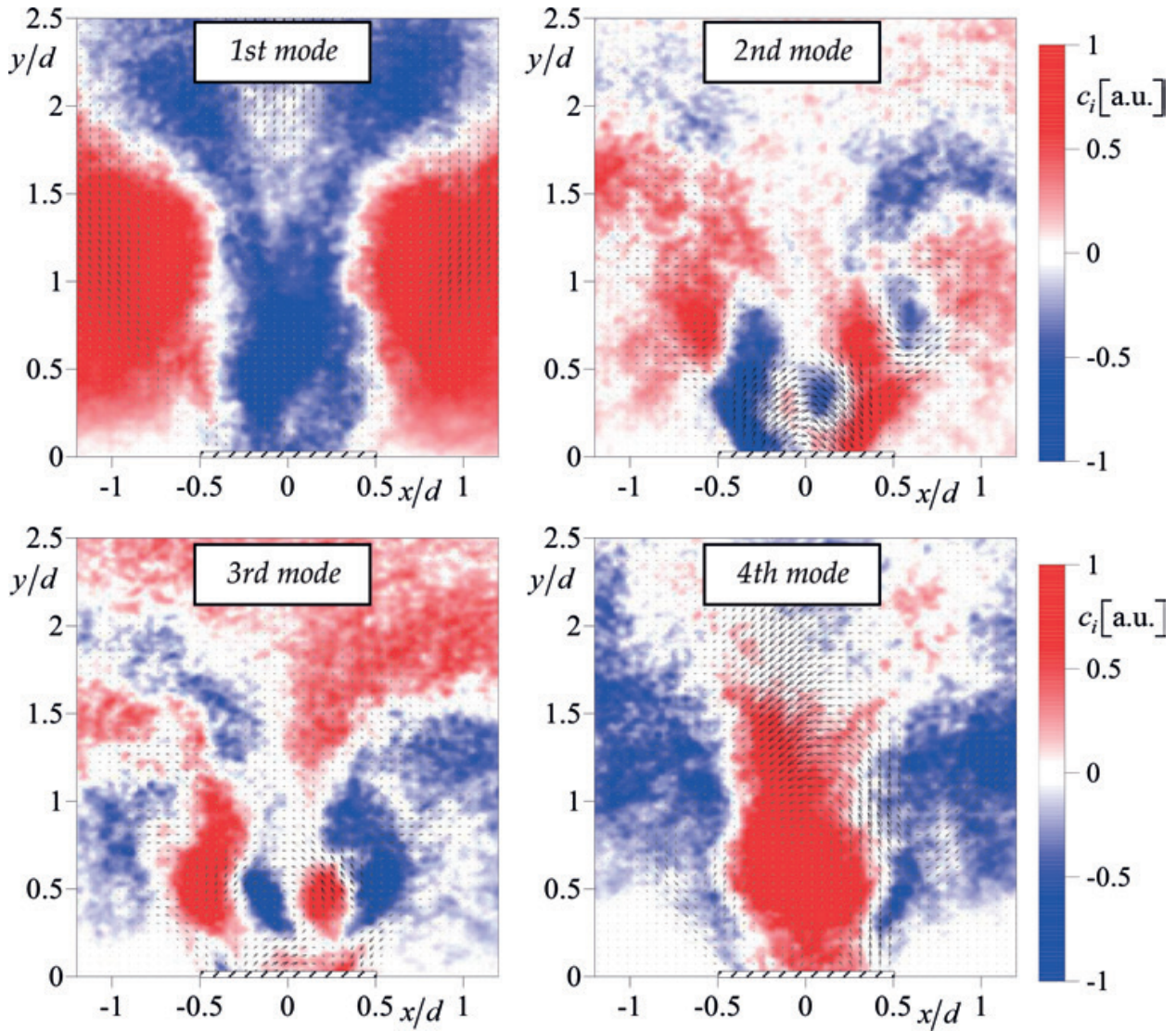

Figure 14. First four POD modes of the velocity fluctuations and conditionally sampled HCHO PLIF fluctuations for a high-swirl fuel-rich flame ($S = 1.0$, $\varphi = 2.5$).

4. Conclusions

Contribution of large-scale coherent structures on regular patterns during turbulent mixing in jet flows with different swirl rates is evaluated on the basis of PIV/PLIF measurements and POD of the velocity snapshots. The main findings are the following:

- For the nonswirling and weakly swirling jet (without permanently present central recirculation zone), toroidal vortices in the outer mixing layer are associated with regular patterns of the concentration fluctuations. For the low-swirl jet, the POD has also revealed variation of the axial velocity in the wake region and transverse movement of the vortex core. Such flow dynamics supports the unsteady vortex breakdown scenario of Oberleithner et al. [12] and is found to be correlated with alternation of the entrainment rate downstream.

- For the strongly swirling jets with vortex breakdown and central recirculation zone, the flow dynamics is related to rotation of a coherent structure, consisting of a pair of large-scale helical vortices. Such coherent structure remains in the considered cases of the fuel-lean and fuel-rich flames. The helical vortices surround the flame front of the lean mixture from both sides and provide regular deformations and stretching of the flame. The outer helical vortex produces ordered concentration structures during the mixing of the jet with the surrounding air and causes large-scale coherent motion of the fuel-rich flame.

Acknowledgements

Conflict of interest

The authors declare no conflict of interest.

Author details

Vladimir Dulin[1,2]*, Aleksei Lobasov[1,2], Dmitriy Markovich[1,2] and Sergey Alekseenko[1,2]

*Address all correspondence to: vmd@itp.nsc.ru

1 Kutateladze Institute of Thermophysics, Siberian Branch of the Russian Academy of Sciences, Novosibirsk, Russia

2 Novosibirsk State University, Novosibirsk, Russia

References

[1] Gupta AK, Lilley DG, Syred N. Swirl Flows. Kent: Abacus Press; 1984. 488 p. DOI: 10.1016/0010-2180(86)90133-1

[2] Fröhlich J, García-Villalba M, Rodi W. Scalar mixing and large-scale coherent structures in a turbulent swirling jet. Flow, Turbulence and Combustion. 2008;**80**(1):47-59. DOI: 10.1007/s10494-007-9121-3

[3] Cozzi F, Coghe A, Sharma R. Analysis of local entrainment rate in the initial region of a isothermal free swirling jets by stereo PIV. Experimental Thermal and Fluid Science. 2018;**94**:281-294. DOI: 10.1016/j.expthermflusci.2018.01.013

[4] Zemtsop CP, Stöllinger MK, Heinz S, Stanescu D. Large-eddy simulation of swirling turbulent jet flows in absence of vortex breakdown. AIAA Journal. 2009;**47**(12):3011-3021. DOI: 10.2514/1.43813

[5] McIlwain S, Pollard A. Large eddy simulation of the effects of mild swirl on the near field of a round free jet. Physics of Fluids. 2002;**14**(2):653-661. DOI: 10.1063/1.1430734

[6] Loiseleux T, Chomaz JM. Breaking of rotational symmetry in a swirling jet experiment. Physics of Fluids. 2003;**15**(2):511-523. DOI: 10.1063/1.1533068

[7] Liang H, Maxworthy T. An experimental investigation of swirling jets. Journal of Fluid Mechanics. 2005;**525**:115-159. DOI: 10.1017/S0022112004002629

[8] Markovich DM, Dulin VM, Abdurakipov SS, Kozinkin LA, Tokarev MP, Hanjalić K. Helical modes in low-and high-swirl jets measured by tomographic PIV. Journal of Turbulence. 2016;**17**(7):678-698. DOI: 10.1080/14685248.2016.1173697

[9] Billant P, Chomaz JM, Huerre P. Experimental study of vortex breakdown in swirling jets. Journal of Fluid Mechanics. 1998;**376**:183-219. DOI: 10.1017/S0022112098002870

[10] Lucca-Negro O, O'doherty T. Vortex breakdown: A review. Progress in Energy and Combustion Science. 2001;**27**(4):431-481. DOI: 10.1016/S0360-1285(00)00022-8

[11] Ruith MR, Chen P, Meiburg E, Maxworthy T. Three-dimensional vortex breakdown in swirling jets and wakes: Direct numerical simulation. Journal of Fluid Mechanics. 2003;**486**:331-378. DOI: 10.1017/S0022112003004749

[12] Oberleithner K, Paschereit CO, Seele R, Wygnanski I. Formation of turbulent vortex breakdown: Intermittency, criticality, and global instability. AIAA Journal. 2012;**50**(7):1437-1452. DOI: 10.2514/1.J050642

[13] Syred N, Chigier NA, Beér JM. Flame stabilization in recirculation zones of jets with swirl. Proceedings of the Combustion Institute. 1971;**13**:617-624. DOI: 10.1016/S0082-0784(71)80063-2

[14] Mourtazin D, Cohen J. The effect of buoyancy on vortex breakdown in a swirling jet. Journal of Fluid Mechanics. 2007;**571**:177-189. DOI: 10.1017/S0022112006002862

[15] Hartung G, Hult J, Kaminski CF, Rogerson JW, Swaminathan N. Effect of heat release on turbulence and scalar-turbulence interaction in premixed combustion. Physics of Fluids. 2008;**20**(3):035110. DOI: 10.1063/1.2896285

[16] Tangirala V, Driscoll JF. Temperatures within non-premixed flames: Effects of rapid mixing due to swirl. Combustion Science and Technology. 1988;**60**(1–3):143-162. DOI: 10.1080/00102208808923981

[17] Bradley D, Gaskell PH, Gu XJ, Lawes M, Scott MJ. Premixed turbulent flame instability and NO formation in a lean-burn swirl burner. Combustion and Flame. 1998;**115**(4):515-538. DOI: 10.1016/S0010-2180(98)00024-8

[18] Schmittel P, Günther B, Lenze B, Leuckel W, Bockhorn H. Turbulent swirling flames: Experimental investigation of the flow field and formation of nitrogen oxide. Proceedings of the Combustion Institute. 2000;**28**(1):303-309. DOI: 10.1016/S0082-0784(00)80224-6

[19] Meier W, Weigand P, Duan XR, Giezendanner-Thoben R. Detailed characterization of the dynamics of thermoacoustic pulsations in a lean premixed swirl flame. Combustion and Flame. 2007;**150**(1–2):2-26. DOI: 10.1016/j.combustflame.2007.04.002

[20] Meier W, Dem C, Arndt CM. Mixing and reaction progress in a confined swirl flame undergoing thermo-acoustic oscillations studied with laser Raman scattering. Experimental Thermal and Fluid Science. 2016;**73**:71-78. DOI: 10.1016/j.expthermflusci.2015.09.011

[21] Konle M, Kiesewetter F, Sattelmayer T. Simultaneous high repetition rate PIV–LIF measurements of CIVB driven flashback. Experiments in Fluids. 2008;**44**(4):529-538. DOI: 10.1007/s00348-007-0411-2

[22] Konle M, Sattelmayer T. Interaction of heat release and vortex breakdown during flame flashback driven by combustion induced vortex breakdown. Experiments in Fluids. 2009;**47**:627-635. DOI: 10.1007/s00348-009-0679-5

[23] Tangermann E, Pfitzner M. Evaluation of combustion models for combustion-induced vortex breakdown. Journal of Turbulence. 2009;**10**(7):1-21. DOI: 10.1080/14685240802592423

[24] Syred N, Beer J. The damping of precessing vortex cores by combustion in swirl generators. Astronautica Acta. 1972;**17**(4):783-801

[25] Schneider C, Dreizler A, Janicka J. Fluid dynamical analysis of atmospheric reacting and isothermal swirling flows. Flow, Turbulence and Combustion. 2005;**74**(3):103-127. DOI: 10.1007/s10494-005-7369-z

[26] Duwig C, Fuchs L. Large eddy simulation of vortex breakdown/flame interaction. Physics of Fluids. 2007;**19**:075103. DOI: 10.1063/1.2749812

[27] Nogenmyr KJ, Fureby C, Bai XS, Petersson P, Collin R, Linne M. Large eddy simulation and laser diagnostic studies on a low swirl stratified premixed flame. Combustion and Flame. 2009;**155**(3):25-36. DOI: 10.1016/j.combustflame.2008.06.014

[28] Day M, Tachibana S, Bell J, Lijewski M, Beckner V, Cheng RK. A combined computational and experimental characterization of lean premixed turbulent low swirl laboratory flames: I. Methane flames. Combustion and Flame. 2012;**159**(1):275-290. DOI: 10.1016/j. combustflame.2011.06.016

[29] Day M, Tachibana S, Bell J, Lijewski M, Beckner V, Cheng RK. A combined computational and experimental characterization of lean premixed turbulent low swirl laboratory flames II. Hydrogen flames. Combustion and Flame. 2015;**162**(5):2148-2165. DOI: 10.1016/j. combustflame.2015.01.013

[30] Mansouri Z, Aouissi M, Boushaki T. Numerical computations of premixed propane flame in a swirl-stabilized burner: Effects of hydrogen enrichment, swirl number and equivalence ratio on flame characteristics. International Journal of Hydrogen Energy. 2016; **41**(22):9664-9678. DOI: 10.1016/j.ijhydene.2016.04.023

[31] Mansouri Z, Aouissi M, Boushaki T. Detached eddy simulation of high turbulent swirling reacting flow in a premixed model burner. Combustion Science and Technology. 2016;**188** (11–12):1777-1798. DOI: 10.1080/00102202.2016.1211888

[32] Lieuwen TC. Unsteady Combustor Physics. Cambridge: Cambridge University Press; 2012. 426 p

[33] Syred N. A review of oscillation mechanisms and the role of the precessing vortex core (PVC) in swirl combustion systems. Progress in Energy and Combustion Science. 2006; **32**(2):93-161. DOI: 10.1016/j.pecs.2005.10.002

[34] Cala CE, Fernandes E, Heitor MV, Shtork SI. Coherent structures in unsteady swirling jet flow. Experiments in Fluids. 2006;**40**(2):267-276. DOI: 10.1007/s00348-005-0066-9

[35] Legrand M, Nogueira J, Lecuona A, Nauri S, Rodríguez PA. Atmospheric low swirl burner flow characterization with stereo PIV. Experiments in Fluids. 2010;**48**(5):901-913. DOI: 10.1007/s00348-009-0775-6

[36] Oberleithner K, Sieber M, Nayeri CN, Paschereit CO, Petz C, Hege HC, Noack BR, Wygnanski I. Three-dimensional coherent structures in a swirling jet undergoing vortex breakdown: Stability analysis and empirical mode construction. Journal of Fluid Mechanics. 2011;**679**:383-414. DOI: 10.1017/jfm.2011.14

[37] Alekseenko SV, Dulin VM, Kozorezov YS, Markovich DM. Effect of high-amplitude forcing on turbulent combustion intensity and vortex core precession in a strongly swirling lifted propane/air flame. Combustion Science and Technology. 2012;**184**(10–11):1862-1890. DOI: 10.1080/00102202.2012.695239

[38] Stöhr M, Boxx I, Carter CD, Meier W. Experimental study of vortex-flame interaction in a gas turbine model combustor. Combustion and Flame. 2012;**159**(8):2636-2649. DOI: 10.1016/ j.combustflame.2012.03.020

[39] Markovich DM, Abdurakipov SS, Chikishev LM, Dulin VM, Hanjalić K. Comparative analysis of low-and high-swirl confined flames and jets by proper orthogonal and dynamic mode decompositions. Physics of Fluids. 2014;**26**(6):065109. DOI: 10.1063/1.4884915

[40] Ceglia G, Discetti S, Ianiro A, Michaelis D, Astarita T, Cardone G. Three-dimensional organization of the flow structure in a non-reactive model aero engine lean burn injection system. Experimental Thermal and Fluid Science. 2014;**52**:164-173. DOI: 10.1016/j.expthermflusci.2013.09.007

[41] Boxx I, Stöhr M, Carter C, Meier W. Temporally resolved planar measurements of transient phenomena in a partially pre-mixed swirl flame in a gas turbine model combustor. Combustion and Flame. 2010;**157**(8):1510-1525. DOI: 10.1016/j.combustflame.2009.12.015

[42] Stöhr M, Sadanandan R, Meier W. Phase-resolved characterization of vortex–flame interaction in a turbulent swirl flame. Experiments in Fluids. 2011;**51**(4):1153-1167. DOI: 10.1007/s00348-011-1134-y

[43] Glassman I. Combustion. 3rd ed. San Diego: Academic Press; 1996. 631 p

[44] Brackmann C, Nygren J, Bai X, Li Z, Bladh H, Axelsson B, Denbratt I, Koopmans L, Bengtsson P-E, Alden M. Laser-induced fluorescence of formaldehyde in combustion using third harmonic Nd:YAG laser excitation. Spectrochimica Acta Part A. 2003;**59**:3347-3356. DOI: 10.1016/S1386-1425(03)00163-X

[45] Syred N, Beer JM. Combustion in swirling flows: A review. Combustion and Flame. 1974;**23**(2):143-201. DOI: 10.1016/0010-2180(74)90057-1

[46] Anacleto PM, Fernandes EC, Heitor MV, Shtork SI. Swirl flow structure and flame characteristics in a model lean premixed combustor. Combustion Science and Technology. 2003;**175**(8):1369-1388. DOI: 10.1080/00102200302354

[47] Fernandes EC, Heitor MV, Shtork SI. An analysis of unsteady highly turbulent swirling flow in a model vortex combustor. Experiments in Fluids. 2006;**40**(2):177-187. DOI: 10.1007/s00348-005-0034-4

[48] Scarano F. Iterative image deformation methods in PIV. Measurement Science and Technology. 2001;**13**(1):R1-R19. DOI: 10.1088/0957-0233/13/1/201

[49] Coudert SJM, Schon J-P. Back-projection algorithm with misalignment corrections for 2D3C stereoscopic PIV. Measurement Science and Technology. 2001;**12**:1371-1381. DOI: 10.1088/0957-0233/12/9/301

[50] Wang GH, Clemens NT. Effects of imaging system blur on measurements of flow scalars and scalar gradients. Experiments in Fluids. 2004;**37**:194-205. DOI: 10.1007/s00348-004-0801-7

[51] Sirovich L. Turbulence and the dynamics of coherent structures. I. Coherent structures. Quarterly of Applied Mathematics. 1987;**45**(3):561-571

[52] Hunt JCR, Wray AA, Moin P. Eddies, stream, and convergence zones in turbulent flows. CTR Report S88. 1988

[53] Broze G, Hussain F. Transitions to chaos in a forced jet: Intermittency, tangent bifurcations and hysteresis. Journal of Fluid Mechanics. 1996;**311**:37-71. DOI: 10.1017/S0022112096002509